THE JOURNAL OF BIOLOGICAL CHEMISTRY
Vol. 278, No. 16, Issue of April 18, pp. 14121–14133, 2003

Printed in U.S.A.

The SNARE Motif Contributes to rbet1 Intracellular Targeting and Dynamics Independently of SNARE Interactions*

Received for publication, January 21, 2003
Published, JBC Papers in Press, February 2, 2003, DOI 10.1074/jbc.M300659200

Ashwini P. Joglekar‡, Dalu Xu‡, Daniel J. Rigotti§¶, Robert Fairman§¶, and Jesse C. Hay‡‖

From the ‡Department of Molecular, Cellular, and Developmental Biology, University of Michigan, Ann Arbor, Michigan 48109 and the §Department of Biology, Haverford College, Haverford, Pennsylvania 19041

The endoplasmic reticulum/Golgi SNARE rbet1 cycles between the endoplasmic reticulum and Golgi and is essential for cargo transport in the secretory pathway. Although the quaternary SNARE complex containing rbet1 is known to function in membrane fusion, the structural role of rbet1 is unclear. Furthermore, the structural determinants for rbet1 targeting and its cyclical itinerary have not been investigated. We utilized protein interaction assays to demonstrate that the rbet1 SNARE motif plays a structural role similar to the carboxyl-terminal helix of SNAP-25 in the synaptic SNARE complex and demonstrated the importance to SNARE complex assembly of a conserved salt bridge between rbet1 and sec22b. We also examined the potential role of the rbet1 SNARE motif and SNARE interactions in rbet1 localization and dynamics. We found that, in contrast to what has been observed for syntaxin 5, the rbet1 SNARE motif was essential for proper targeting. To test whether SNARE interactions were important for the targeting function of the SNARE motif, we used charge repulsion mutations at the conserved salt bridge position that rendered rbet1 defective for binary, ternary, and quaternary SNARE interactions. We found that heteromeric SNARE interactions are not required at any step in rbet1 targeting or dynamics. Furthermore, the heteromeric state of the SNARE motif does not influence its interaction with the COPI coat or efficient recruitment onto transport vesicles. We conclude that protein targeting is a completely independent function of the rbet1 SNARE motif, which is capable of distinct classes of protein interactions.

Soluble *N*-ethylmaleimide-sensitive factor attachment protein receptor (SNARE)[1] complexes bridge opposing membrane bilayers and appear to mediate specific membrane fusion in the endomembrane system (1, 2). Although SNARE complexes appear to represent a universal membrane fusion machine, their role in determining the specificity of intracellular membrane fusion is still being established (3, 4). Each SNARE complex characterized to date appears to consist of a thermostable parallel helix bundle composed of four heptad repeat-containing SNARE motifs (5–9). Because the parallel SNARE motifs are anchored via transmembrane domains continuous with the carboxyl end of the SNARE motifs, the amino-to-carboxyl-terminal "zippering up" of the vesicle (v-) SNARE motif with the target membrane (t-) SNAREs draws the two membranes into close apposition and apparently drives lipid mixing and fusion between the opposing bilayers (3).

Although most of the residues that interact in the core of SNARE helix bundles are hydrophobic, one well conserved interior layer of polar residues lies at the center of each bundle. Interestingly, most SNAREs structurally related to syntaxin 1A and SNAP-25 contain a glutamine at this conserved "zero layer" position (called "Q-SNAREs"), whereas SNAREs related to VAMP 2 contain an arginine at this position ("R-SNAREs") (10). Based upon protein profiling analysis, Q-SNAREs can be further subdivided into Q_A-SNAREs related to syntaxin and Q_B- and Q_C-SNAREs related to the amino- and carboxyl-terminal SNARE motifs of SNAP-25, respectively (11). Notably, all of the characterized SNARE complexes and fusogenic subsets of SNAREs in liposome fusion to date contain one each of the Q_A-, Q_B-, Q_C-, and R-SNARE motifs. Several studies have investigated the function of this conserved central layer; although aspects of its composition are essential for proper SNARE function, its precise role(s) in complex formation, membrane fusion and/or SNARE recycling still remains unclear (reviewed in Ref. 2).

In several systems it appeared that a reproducible pattern emerged concerning the subunit organization of SNARE four-helix bundles. The exocytic SNARE complex is well known to be comprised of a set of three interacting Q-SNARE helices anchored on one membrane that form a binding site for an R-SNARE helix anchored on an opposing membrane. In the endosomal complex, now known in atomic detail, the positions occupied by the amino- and carboxyl-terminal SNAP-25 helices in the exocytic complex are held by the Q_B-SNARE vti1b and the Q_C-SNARE syntaxin 8, respectively, whereas the R-SNARE VAMP 8 superimposes upon the VAMP 2 position, and syntaxin 7 is spatially equivalent to syntaxin 1A (6, 7). Thus, this crystal structure demonstrated that SNARE motif positions are highly superimposable between complexes and that the structural roles of the Q_A-, Q_B-, Q_C-, and R-SNARE motifs are likely to be conserved, at least between the synapse and endosomes. A similar assumption was made about the ER/Golgi quaternary complex because the R-SNARE sec22b bound strongly only to the *combination* of the Q_A-, Q_B-, and Q_C-SNAREs syntaxin 5, membrin, and rbet1. Thus, sec22b appeared to play an analogous role to VAMP 2 and was mod-

* This work was supported by National Institutes of Health Grant GM59378 (to J. C. H.). The costs of publication of this article were defrayed in part by the payment of page charges. This article must therefore be hereby marked "*advertisement*" in accordance with 18 U.S.C. Section 1734 solely to indicate this fact.

¶ Supported by National Science Foundation Grant MCB-0211754.

‖ To whom correspondence should be addressed: Dept. of Molecular, Cellular, and Developmental Biology, University of Michigan, 830 North University Ave., Ann Arbor, MI 48109. Tel.: 734-647-6662; Fax: 734-647-0884; E-mail: jessehay@umich.edu.

[1] The abbreviations used are: SNARE, soluble *N*-ethylmaleimide-sensitive factor attachment protein receptor; v-, vesicle; t-, target membrane; ER, endoplasmic reticulum; GST, glutathione *S*-transferase; BSA, bovine serum albumin; AU, analytical ultracentrifugation; BFA, brefeldin A; GTPγS, guanosine 5′-3-*O*-(thio)triphosphate; SNAP, soluble *N*-ethylmaleimide-sensitive factor attachment protein; NRK, normal rat kidney; CFP, cyan fluorescent protein; VTC, vesicular tubular cluster; ARF, ADP ribosylation factor; GAP, GTPase-activating protein.

eled to oppose the Q-SNAREs syntaxin 5, membrin, and rbet1 in ER/Golgi membrane fusion events (9, 12). However, results from *in vitro* liposome fusion with purified recombinant yeast ER/Golgi SNAREs suggested a different model of the putative first fusion event in the secretory pathway, because fusion did not occur when Sec22p opposed Sed5p, Bos1p, and Betlp on liposomes (13). Instead, a membrane fusion signal was generated only when Bet1p opposed Sec22p, Bos1p, and Sed5p. This result was interpreted to mean that *in vivo*, Bet1p is the V-SNARE that opposes a t-SNARE complex composed of Sec22p, Bos1p, and Sed5p. According to this interpretation, the spatial organization and membrane topology of structurally related SNAREs in membrane fusion complexes is not conserved and instead must be determined on a case-by-case basis.

Because of the specific intracellular localizations displayed by SNAREs and because their specific localizations and interactions appear to encode at least one layer of specificity in vesicle transport reactions (3), there has been considerable interest in understanding the intracellular targeting determinants within the SNAREs themselves. The results have been surprisingly variable. In the simplest cases, the subcellular localization information is apparently contained entirely within the transmembrane domain and may even be a simple function of transmembrane domain length. This is the case for the plasma membrane SNAREs syntaxin 3 and 4 as well as for the ER/Golgi syntaxin 5, whose transmembrane domains are sufficient for proper localization (14–16). Syntaxin 5 may also contain additional targeting information within its cytoplasmic domain, although results differ. On the other hand, syntaxin 6, which follows a complex itinerary that includes steady-state localization to the *trans*-Golgi network and endosomes (17) and undergoes constitutive cycling to the plasma membrane, appears to be targeted by two distinct determinants within its cytoplasmic domain (18), one within the SNARE motif and the other within its amino-terminal domain, now known to represent a three-helix bundle (19). At least two other syntaxin family members also contain essential localization determinants within their cytoplasmic domains (16). Although it was speculated that the targeting via these determinants was accomplished by protein interactions, the binding partners required for localization were not identified. Similarly, the SNARE motif was required for efficient VAMP 2 recruitment onto synaptic vesicles (20). In this case, mutagenesis revealed that the capacity for synaptic SNARE interactions did not correlate with targeting to synaptic vesicles, implicating other potential SNARE motif binding partners for targeting (20, 21). Very recently, the mammalian R-SNARE ykt6 was demonstrated to be targeted to a very specific yet undescribed vesicular localization by virtue of its profilin-like amino-terminal domain, completely independently of its SNARE motif or hydrophobic anchor in membranes (22). Thus, as of yet SNARE targeting does not appear to follow a clear set of rules and may instead utilize several distinct classes of protein and/or membrane interactions.

One question that has not been explored is whether SNAREs are trafficked individually or as complexes. This would be particularly relevant to t-SNAREs that undergo constitutive cycling, for example within the Golgi, between the ER and Golgi or between the Golgi and endosomes. Some cycling SNAREs may contain their own intrinsic targeting signals, whereas others could depend upon interactions with these SNAREs for their targeting. If Q-SNARE complexes are indeed an important intermediate in SNARE complex assembly, then one might expect these complexes to be efficiently recruited onto newly forming vesicles. On the other hand, one might expect used or aberrant SNARE complexes to be excluded from newly forming vesicles.

Targeting determinants of the dynamically localized ER/Golgi Q_C-SNARE Bet1p and its rat ortholog rbet1 have not been defined. rbet1 is a small SNARE consisting of a carboxyl-terminal transmembrane domain attached to a 95-amino acid cytoplasmic domain with no predicted structure other than the SNARE motif of residues 27–90. In mammals, rbet1 displays a steady-state localization to VTCs and early Golgi and undergoes rapid constitutive cycling between the ER and Golgi (23). Direct interactions between the yeast Bet1p SNARE motif and the COPI and COPII coat machinery have been described (24, 25). Furthermore, interactions of Bos1p and Sec22p with COPII components were sufficient to produce a 3–4-fold enrichment of the SNAREs in COPII vesicles budded from chemically defined liposomes (26). Thus, interactions between the rbet1 SNARE motif and COP coats could be important for its steady-state localization and for its constitutive ER/Golgi cycling. On the other hand, correct recruitment to budding vesicles may be more complex *in vivo* than simple interactions with coats; for example, it may also involve determinants that localize the protein to vesicle budding sites or membrane domains. This may be the case for the erv41p-erv46p complex, another rapidly cycling vesicle membrane protein (27). Recent findings in yeast indicated that ARF-GAP bound transiently to the Bet1p SNARE motif *in vitro* and induced a conformational state required for its interaction with COPI machinery (25). Because the known conformational states for SNARE motifs are unstructured coils and helical bundles, one suggestion was that ARF-GAP may facilitate Bet1p hetero- or homo-oligomeric bundling and that oligomeric bundles are the preferred substrate for coat binding and uptake into vesicles. These speculations highlight our lack of information about the role of the SNARE motif and SNARE protein interactions in the targeting, dynamics, and life cycle of the SNAREs themselves.

Using purified SNAREs and simple protein interaction assays and mutagenesis, we have further investigated the organization of the ER/Golgi quaternary complex *in vitro*. In contrast to results with liposome fusion, our results demonstrate that membrin and rbet1 play the structural roles of t-SNAREs, with membrin being spatially analogous to the amino-terminal helix of SNAP-25 and rbet1 occupying a position very similar to the carboxyl-terminal helix of SNAP-25. In addition, we demonstrated the importance to SNARE complex assembly of a conserved salt bridge on the surfaces of the synaptic and ER/Golgi SNARE complexes. In a second set of experiments, we examined the potential role of the rbet1 SNARE motif and SNARE interactions in rbet1 localization and dynamics. We found that, in contrast to what has been observed for its binding partner syntaxin 5, the rbet1 SNARE motif was absolutely essential for proper targeting. For a clean test of the role of SNARE interactions in rbet1 targeting or dynamics, we created charge repulsion mutant rbet1 K47D at the conserved salt bridge position that rendered rbet1 defective for heteromeric SNARE interactions *in vivo*. Interestingly, the steady-state localization of rbet1 K47D was indistinguishable from wild type. Furthermore, the intracellular dynamics of the mutant, its interactions with the COPI machinery, and its recruitment to coated vesicles were all indistinguishable from wild type. We conclude that the SNARE motif but not SNARE interactions is essential for the targeting and dynamics of rbet1.

EXPERIMENTAL PROCEDURES

Antibodies—Monoclonal and affinity-purified polyclonal anti-SNARE antibodies were described previously (23, 28). An anti-hexahistidine monoclonal antibody was obtained from Sigma. β-COP antiserum was raised in a rabbit by injection of the peptide CKKEAGELKPEEEITVGPVQK conjugated to keyhole limpet hemocyanin. p24α2 anti-

serum was raised in a rabbit by injection of the peptide CQMRHLKSFFEAKKLV conjugated to keyhole limpet hemocyanin. An anti-rsec23 antibody (which recognizes all isoforms) was raised in a rabbit against the peptide CQQNEERDGVRFSWNVWPSSR conjugated to keyhole limpet hemocyanin and then affinity-purified using the peptide. Glucosidase IIα and protein disulfide isomerase antibodies were purchased from Stressgen (catalog numbers VAP-PT034 and SPA-890, respectively). Anti-calnexin was from Dr. Ari Helenius, and anti-GM130 was from Dr. Martin Lowe. Anti-syntaxin 6 monoclonal antibody (clone 3A10) was from Drs. Richard Scheller and Jason Bock.

Expression and Purification of ER/Golgi SNAREs—The following bacterially expressed protein constructs were either described previously (9) or created for this study. GST-membrin encoded essentially the full-length protein (amino acids 2–212) including the transmembrane domain and was mutated at residue 139 with a QuikChange kit from Stratagene. GST-syntaxin 5 included the entire cytoplasmic domain of the smaller 34-kDa syntaxin 5 isoform (residues 55–333 of the entire syntaxin 5 open reading frame); however, we used a natural internal thrombin cleavage site within this construct (9) to produce a fragment containing just the SNARE motif, residues 252–333 for binding studies. GST-rbet1 encoded the entire cytoplasmic domain (residues 1–95) and was mutated using the QuikChange kit to produce the rbet1 mutations employed in the experiments. GST-SNAP-25 encoded either the entire protein (residues 1–206), the amino-terminal SNARE motif (residues 1–93), or the carboxyl-terminal SNARE motif (residues 120–206). We also employed three hexahistidine-tagged constructs: mouse sec22b cytoplasmic domain (residues 2–196), yeast Sec22p cytoplasmic domain (residues 2–193), and rbet1 cytoplasmic domain (residues 2–95). The mouse sec22b construct was mutagenized with the QuikChange kit as indicated in the text. All of the constructs and mutants were verified by sequencing at the University of Michigan DNA sequencing core.

For binding studies, the SNARE proteins were purified as described earlier (9). In short, *Escherichia coli* cultures were resuspended in French press buffer (50 mM Tris, pH 8.0, 0.1 M NaCl, 1 mM EDTA, 0.05% Tween 20, 1 mM dithiothreitol, 2 μg/ml leupeptin, 4 μg/ml aprotinin, 1 μg/ml pepstatin A, and 1 mM phenylmethylsulfonyl fluoride) (for His_6-containing constructs, we used the same medium without dithiothreitol), lysed by French press, and then centrifuged at 20,000 $\times$ *g* for 20 min, and the supernatant (S1) was recovered. For His_6-sec22b, GST, GST-rbet1, and GST-SNAP-25 constructs, the S1 was immediately centrifuged at 100,000 $\times$ *g* for 45 min, and the supernatant was collected (S2). For GST-syntaxin 5 (55- 333), the S1 was adjusted to 0.35% sodium sarkosyl, mixed gently for 30 min, and then supplemented with 1% Triton X-100 and 10% glycerol. After centrifugation at 100,000 $\times$ *g* for 45 min, the supernatant was collected. For GST-membrin, the S1 was centrifuged at 100,000 $\times$ *g* for 45 min, the supernatant (S2) was discarded, and the pellet (P2) was homogenized in the original volume of French press buffer. This was treated with sarkosyl, glycerol, and Triton X-100 and centrifuged as above, and the 100,000 $\times$ *g* supernatant was retained. All of the final 100,000 $\times$ *g* supernatants were then purified on columns of either glutathione-Sepharose (GST constructs) or Ni^{2+}-nitrilotriacetic acid-agarose (His_6 constructs). Purified fractions eluted with glutathione were cleaved with thrombin in the case of GST fusion proteins. The purified, cleaved proteins were dialyzed into Buffer A (20 mM Hepes, pH 7.2, 0.15 M KCL, 2 mM EDTA, 5% glycerol), supplemented with protease inhibitors, and stored at −80 °C. The proteins were quantified by comparison with BSA standards on Coomassie-stained SDS gels, employing an Agfa Arcus 1200 flatbed scanner and Kodak 1D Image gel analysis software.

rbet1 employed for analytical ultracentrifugation (AU) experiments was purified by more rigorous procedures. The first stages of purification were identical to above. However, after elution from glutathione-Sepharose, GST-rbet1 fusion proteins were further purified by anion exchange chromatography on MonoQ (Amersham Biosciences). After elution with a continuous KCl gradient, the peak of the desired protein was pooled and cleaved with thrombin, diluted 2-fold with low salt buffer, and passed over a column of Q-Sepharose to retain GST and residual fusion protein. The flow-through from the Q-Sepharose, containing cleaved rbet1, was concentrated using a YM-3 membrane on an Amicon stirred cell concentrator and then further purified by velocity gradient fractionation as described earlier (9). The final homogeneous rbet1 was dialyzed into 20 mM Tris, pH 8.0, for AU analysis.

Binding Assays—All of the binding incubations were conducted in buffer A containing 0.1% Triton X-100. For solution binding assays, 300-μl reactions containing ~2 μM of each protein were incubated for varying time periods (see each figure legend) on ice, 250 μl of which was injected onto a 24-ml Superdex 200 gel filtration column (Amersham Biosciences) run in Buffer A containing 0.1% Triton X-100 and 30 μg/ml BSA. Individual column fractions were either analyzed directly by SDS-PAGE and Western blotting or were precipitated with acetone prior to gel and Western analysis.

For the binary and ternary bead binding assays, a typical binding reaction consisted of 20 μl of 20 mg/ml BSA, 20 μl of 50% glutathione-Sepharose beads containing ~124 pmol (620 nM final concentration in binding reaction) of the immobilized protein, and varying amounts of the soluble binding partners in a final volume of 200 μl of Buffer A plus 0.1% Triton X-100. The binding reactions were incubated for 1 h at 4 °C with constant agitation, and then the beads were washed three times with Buffer A containing 0.1% BSA in the case of binary binding reactions and Buffer A plus 0.1% Triton X -100 in the case of ternary bead binding assays. The beads were resuspended in denaturing sample buffer and analyzed by SDS-PAGE followed by Western blotting, scanning, and quantitation.

Immunofluorescence Microscopy—NRK cells seeded on coverslips were transfected with wild type Myc-rbet1 or Myc-rbet1 K47D using LipofectAMINE 2000 reagent (Invitrogen). In some experiments the cells were co-transfected with a commercial CFP-tagged galactosyltransferase localization domain construct (Living Colors CFP-Golgi from Clontech). For brefeldin A treatment, the cells were incubated for 60 min in growth medium containing 10 μg/ml of brefeldin A (Calbiochem). To allow the BFA-treated cells to recover from treatment, the BFA containing medium was removed, and the cells were washed twice with non-BFA containing growth medium and then incubated with fresh growth medium for the indicated amounts of time. For the low temperature treatment, the cells were incubated at 15 °C in precooled growth medium for the indicated amounts of time. To fix cells for microscopy, the growth medium was removed, and the cells were incubated with 2% paraformaldehyde in 0.1 M sodium phosphate, pH 7.0, followed by quenching twice for 10 min each with 0.1 M glycine in phosphate-buffered saline. The cells were permeabilized by incubation with permeabilization solution (0.4% saponin, 1% BSA, and 2% normal goat serum in phosphate-buffered saline) for 15 min. They were then incubated with permeabilization solution containing the primary antibody for 1 h at room temperature and washed three times with permeabilization solution, and the purified fluorescently labeled secondary antibody (Jackson Immunoresearch) in permeabilization solution was added to the cells for 30 min. The cells were finally washed three times with permeabilization solution and mounted in Vectashield medium (Vector Labs) on glass slides. Microscopy was conducted on a Nikon E800 epifluorescence microscope with Texas Red and fluorescein filter sets, a Hamamatsu Orca II camera, and Improvision Openlab software.

Immunoprecipitation Experiments—NRK cells were transfected with either wild type Myc-rbet1 or Myc-rbet1 K47D constructs. Twenty-four hours after transfection, the cells were washed twice with cold phosphate-buffered saline and solubilized in KCl Buffer (20 mM Hepes, pH 7.2, 0.1 M KCl, 2 mM EGTA, 2 mM EDTA) containing 1.0% Triton X-100, 1 mM dithiothreitol, 2 μg/ml leupeptin, 4 μg/ml aprotinin, 1 μg/ml pepstatin A, 1 mM phenylmethylsulfonyl fluoride, 5 mM $MgCl_2$, and 1 mM GTPγS. The extract obtained was centrifuged at 100,000 $\times$ *g* for 30 min. The clarified supernatants were processed for immunoprecipitation using specific antibodies and protein A beads. After a 2-h incubation with the extracts, the beads were washed with Buffer A containing 0.1% Triton X-100, and the proteins were solubilized with SDS-PAGE sample buffer. The immunoprecipitates and the starting extracts were then analyzed by SDS-PAGE and immunoblotting.

In Vitro Vesicle Generation—Rat liver cytosol was prepared by homogenization of a fresh liver in four volumes of 25/125 (25 mM Hepes, 125 mM potassium acetate, pH 7.2) containing 1 mM dithiothreitol, 1 mM 4-(2-aminoethyl)benzenesulfonyl fluoride, 2 μg/ml leupeptin, 4 μg/ml aprotinin, and 2 μg/ml pepstatin, using a Potter-Elvejem homogenizer in a drill press. After an initial centrifugation at 20,000 $\times$ *g* for 20 min, the supernatant was further centrifuged at 100,000 $\times$ *g* for 1 h. The top lipid layer was discarded, and the remaining supernatant was desalted into 25/125 using Sephadex G-25 or dialyzed against 25/125 for 4 h at 4 °C. Cytosol aliquots were snap frozen and stored at −80 °C. For budding of vesicles, one 10-cm plate of just-confluent NRK cells were scraped from the plate with a rubber policeman into buffer 50/90 (50 mM Hepes, pH 7.2, 90 mM potassium acetate). The cells were then washed once with 50/90, resuspended in a final volume of 100 μl of 50/90, and added to a budding reaction in a total volume of 800 μl containing buffer 25/125 supplemented with 2.5 mM MgOAc, 5 mM EGTA, 1.8 mM $CaCl_2$, 1 mM ATP, 5 mM creatine phosphate, 5 units/ml creatine phosphokinase, and 200 μl of rat liver cytosol. Budding reactions were incubated at 32 °C for 90 min and stopped on ice for 5 min, and the cells were removed with a 4,000 $\times$ *g* centrifugation for 1 min. Then either the

supernatant was directly subjected to a 100,000 × *g* centrifugation and the pellet was subjected to immunoblotting, or the supernatant was fractionated by iodixanol gradient prior to immunoblot analysis. For gradient analysis, the 4,000 × *g* supernatants from budding reactions (800 μl) were layered on top of 150 μl of 7% iodixanol (diluted with Optiprep diluent: 0.25 M sorbitol, 10 mM Hepes, 1 mM EDTA, pH 7.4) layered on top of 300 μl of 50% iodixanol and centrifuged at 100,000 × *g* for 40 min. The top 800 μl was then aspirated, and the remaining 450 μl was mixed and bottom-loaded under a 5–25% continuous iodixanol gradient. After a 90-min 100,000 × *g* centrifugation, the gradient was fractionated from the top, diluted with Optiprep diluent, and subjected to a 120,000 × *g* centrifugation for 1 h. The pellets were then analyzed by immunoblotting.

Analytical Ultracentrifugation—The experiments were performed at 4 °C with a Beckman Optima XL-A analytical ultracentrifuge equipped with 12-mm path length, six-channel, charcoal-filled Epon cells and quartz windows, using rotor speeds of 30,000, 35,000, and 40,000 rpm. rbet1 was dialyzed into 20 mM Tris, pH 8.0; the loading concentration of rbet1 was 1 μM. Partial specific volume and solution density were calculated using the program Sednterp (29). The data were globally fit with a single-species model with the molecular mass treated as a fitting parameter. The WinNonLin (V1.060) program from the Analytical Ultracentrifugation Facility at the University of Connecticut (Storrs, CT) was used for the fitting analysis.

RESULTS

Membrin and rbet1 Play Structural Roles Similar to the First and Second Helices of SNAP-25, Respectively—The purified recombinant ER/Golgi SNAREs syntaxin 5, membrin, rbet1, and sec22b appeared to form a quaternary complex with each protein contributing a single SNARE motif (9). We hypothesized that the ER/Golgi complex formed a four-helix bundle with similar structural and regulatory features to the synaptic SNARE complex (5). Because the synaptic and late endosomal four-helix bundles display virtually superimposable structures with the corresponding SNARE motifs in each family (Q_A, Q_B, Q_C, and R) occupying the same positions in the two complexes, it seemed likely that the ER/Golgi quaternary complex would also display this conserved organization. However, a liposome fusion assay employing yeast ER/Golgi SNAREs indicated a radically different arrangement, with the R-SNARE Sec22p acting as part of a t-SNARE complex and the Q_C-SNARE Bet1p opposing the t-SNARE in the v-SNARE position (13). We wondered whether these results were indicative of a true difference in the structural roles of the four classes of SNARE motifs in the ER/Golgi SNARE complex. To address this we performed substitution experiments using purified proteins to determine whether SNARE motifs from the synaptic complex could assemble with ER/Golgi SNAREs and, if so, which helices in the two complexes would be equivalent. We first asked whether SNAP-25 could replace any of the Q-SNAREs syntaxin 5, membrin, or rbet1 in the formation of a hybrid ER/Golgi SNARE complex. We examined the formation of complexes in solution using gel filtration to resolve high molecular mass complexes from monomers. Under these conditions, sec22b can only participate in the formation of a quaternary complex and does not exhibit binary or ternary interactions with ER/Golgi Q-SNAREs (9). Therefore, we used the appearance of sec22b in the high molecular mass fractions as an indicator of the formation of a four-helical complex. As shown in Fig. 1*A*, SNAP-25 can substitute for both membrin and rbet1 (*top two panels*). The high molecular mass complex(es) containing SNAP-25, syntaxin 5, and sec22b appear to involve all three proteins because in control reactions omitting SNAP-25 or syntaxin 5, sec22b eluted in the monomeric range (Fig. 1*A*, *third* and *fourth panels*). Importantly, SNAP-25 would not substitute for other pairwise combinations, including syntaxin 5/membrin and syntaxin 5/rbet1 (Fig. 1*A*, *bottom two panels*). Note that the gel filtration size under these conditions does not accurately predict the number of molecules in a SNARE complex, because the

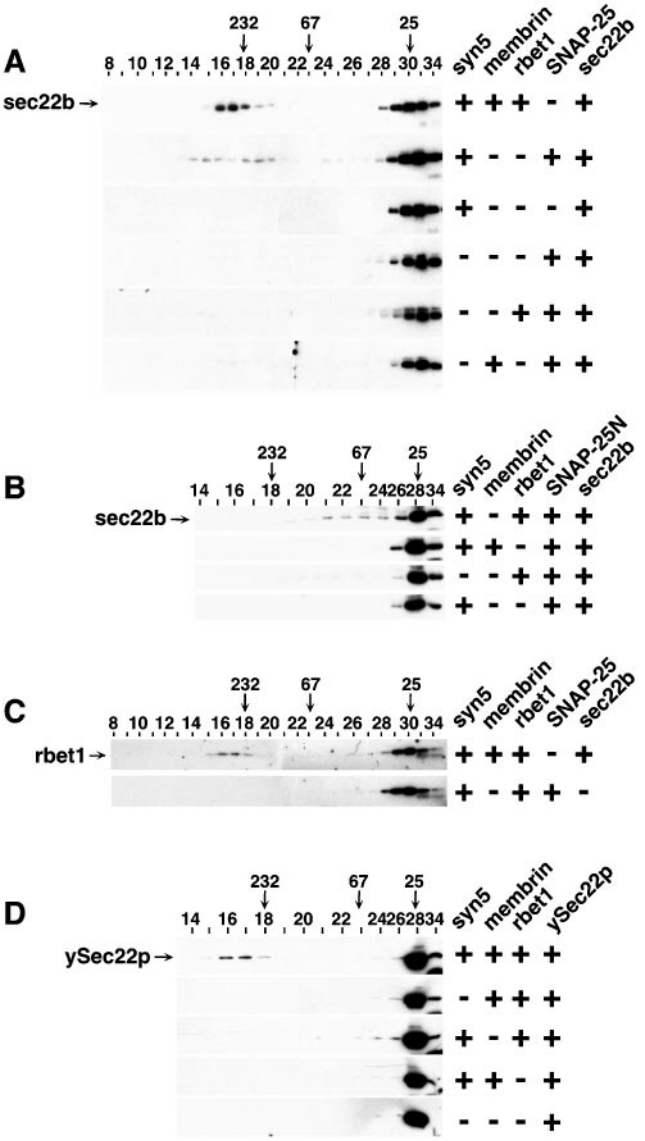

FIG. 1. **Substitutions of SNAP-25 helices delineate corresponding helices in the ER/Golgi SNARE complex.** Purified, bacterially produced recombinant SNAREs were mixed in the indicated combinations and incubated overnight at 4 °C. Each protein had a final concentration of ~2 μM and was used at an identical concentration in every reaction. Incubated binding reactions were gel-filtered on Superdex 200, and the individual fractions were immunoblotted for the protein indicated to the *left* of each panel. In *B* and *D*, the sample labeled *28* is a pool of 28, 30, and 32; the sample labeled *34* is a pool of 34, 36, and 38. In *A* and *C*, fractions were analyzed individually. The elution positions of globular marker proteins are indicated *above* the fraction numbers.

complexes contain an unknown quantity of bound Triton X-100, and the aggregation state of SNARE complexes is not well understood. We do not know why the hybrid SNAP-25 complex displays a biphasic distribution (Fig. 1*A*, *second panel*) but speculate that the complex may be present in two distinct aggregation states. This could be due to the two SNAP-25 SNARE motifs participating in different individual SNARE complexes (30). In summary, the results of Fig. 1*A* suggest that there is a high degree of structural conservation between the two complexes and that membrin and rbet1 occupy positions in the ER/Golgi complex that approximate the positions of SNAP-25 in the synaptic complex.

We next sought to determine which of the Q-SNAREs, membrin and rbet1, mimics the first and which the second of the two SNAP-25 SNARE motifs (referred to as SNAP-25N and SNAP-

25C, respectively). Based upon protein profiling techniques, membrin appears more closely related to SNAP-25N, and rbet1 appears more closely related to SNAP-25C (11). Indeed, as shown in Fig. 1*B* (*top panel*), a SNAP-25N fragment encoding residues 1–93 appears to substitute for membrin in the quaternary complex, the formation of which is reflected by the appearance of sec22b in the high molecular mass fractions. This shift is not observed in the reaction containing syntaxin 5, sec22b, membrin, and SNAP-25N, indicating that only membrin, and not rbet1, can be "replaced" by SNAP-25N (Fig. 1*B*, *second panel*). These data indicate that the structural role of membrin in the ER/Golgi quaternary complex may be similar to that of the first SNAP-25 helix in the synaptic SNARE complex. Curiously, the hybrid complex containing syntaxin 5, SNAP-25N, rbet1, and sec22b had a gel filtration size significantly smaller than the native ER/Golgi complex (~100 kDa *versus* ~300 kDa; compare fraction numbers between Fig. 1*A*, *top panel*, and Fig. 1*B*, *top panel*); this could be due to an altered oligomerization state of this complex. However, the experiment in Fig. 1*B* establishes that the hybrid complex indeed contains all four of the participant proteins, because removing rbet1 or syntaxin 5 from the incubations abolishes the high molecular mass sec22b-containing complexes (Fig. 1*B*, *bottom two panels*) and sec22b does not associate with syntaxin 5 and rbet1 on its own (9). Unfortunately, we could not obtain clean substitution data for the second SNAP-25 helical domain using this technique, because the SNAP-25C construct displayed binary interactions with sec22b (data not shown). In summary, the SNAP-25 and SNAP-25N substitutions indicate that in the ER/Golgi quaternary complex, the membrin position is similar to that of SNAP-25N and that rbet1 therefore most likely resembles SNAP-25C.

It is important to note that although equimolar concentrations of SNAP-25 constructs, membrin, rbet1, and sec22b were used in the experiments, there was a substantially lower yield of the hybrid complexes than the native ER/Golgi complex. In addition, overnight incubations were required to produce detectable hybrid complex, whereas the ER/Golgi complex is readily detectable in 1–2 h (not shown). Hence, although the experiment suggests structural relatedness, it is also consistent with some limited specificity between cognate SNAREs in solution.

We next tested whether rbet1 could behave like a v-SNARE in its binding characteristics. If rbet1 could behave like a v-SNARE, it might be expected to form a complex with syntaxin 5 and the two SNAP-25 helices, which by definition play the role of t-SNARE. Put differently, SNAP-25 would be expected to substitute for membrin and sec22b. As shown in Fig. 1*C*, no detectable high molecular mass rbet1-containing complex is formed from rbet1, SNAP-25 and syntaxin 5 (*bottom panel*), but an rbet1-containing complex is readily detectable in a reaction involving all four ER/Golgi proteins (*top panel*). This experiment is consistent with the hypothesis that in the ER/Golgi complex, rbet1 occupies the position of a SNAP-25 helix and therefore cannot co-exist in a hybrid complex with SNAP-25. On the other hand, sec22b readily binds to the hybrid syntaxin 5-SNAP-25 t-SNARE (Fig. 1*A*).

We also considered the possibility that the yeast ER/Golgi SNAREs simply had very different binding characteristics from their mammalian counterparts. For example, perhaps yeast Sec22p is part of a t-SNARE complex, whereas mammalian sec22b acts in a v-SNARE mode. We tested this possibility by preparing purified yeast Sec22p and asking whether it behaved differently from the mammalian sec22b in binding reactions with the mammalian Q-SNAREs syntaxin 5, membrin, and rbet1. As shown in Fig. 1*D*, yeast Sec22p, just like sec22b, formed a quaternary complex with the three Q-SNAREs (*top panel*). Furthermore, like sec22b, yeast Sec22p interacted only with the combination of syntaxin 5, membrin, and rbet1 and not with any other combination (Fig. 1*D*, *second*, *third*, and *fourth panels*). The fact that yeast Sec22p behaves indistinguishably from sec22b and forms a high affinity quaternary complex with syntaxin 5, rbet1, and membrin and did not form detectable t-SNARE complexes with any subset of them is inconsistent with this yeast protein playing a fundamentally different structural role in SNARE complexes. For example, if Sec22p were a syntaxin light chain as suggested (13), then it would not have been compatible with membrin or rbet1, both of which appear to play that role (Fig. 1, *A* and *B*). To the contrary, yeast Sec22p was entirely dependent upon the presence of both of those proteins for a stable interaction.

Conserved Interchain Interactions between rbet1 and sec22b—Based upon the above substitution experiments, our working hypothesis is that the four ER/Golgi SNARE motifs are arranged nearly superimposably over the synaptic core complex, using these chain correspondences: syntaxin 5 and syntaxin 1A; membrin and SNAP-25N; rbet1 and SNAP-25C; and sec22b and VAMP 2. If corresponding chains do indeed occupy the same space in the two complexes, then specific interchain interactions, for example the salt bridges between the SNAP-25C helix and VAMP, may be conserved in the ER/Golgi complex. In the synaptic complex, there are ionic interactions on the surface of the bundle between SNAP-25 Arg^{61} and VAMP 2 Glu^{41} and between SNAP-25 Asp^{86} and VAMP 2 Arg^{66} (5). If rbet1 and sec22b are aligned with these chains using the zero layer Q and R to determine the location of the layers and a superimposable backbone structure is assumed, then both salt bridges would be potentially conserved, with rbet1 Lys^{47} interacting with sec22b Asp^{144} and rbet1 Asp^{72} in contact with sec22b Lys^{169} (an alignment is shown for reference in Fig. 2*A*). Based upon the protein profiling analysis structural categorization of SNARE motifs (11), the vast majority of SNARE complexes would have conserved salt bridges at those positions. On the other hand, if rbet1 were modeled in the structural role of VAMP 2, as suggested by the liposome fusion studies, then ionic residues would not be present at those positions.

To further explore and confirm the organization of the ER/Golgi quaternary complex, we mutated an rbet1 residue, Lys^{47}, that potentially interacts with sec22b Asp^{72} on the surface of the bundle. We produced two mutations, K47E and K47D, to potentially create ionic repulsion with sec22b Asp^{72} and tested their effects on quaternary complex formation relative to wild type proteins under identical conditions. As seen in Fig. 2*B* (*first*, *second*, and *third panels*), K47E resulted in 49% less complex formation compared with wild type, whereas surprisingly, K47D was completely defective in quaternary SNARE complexes. One likely explanation for the dramatic difference between the two mutations was that because of the highly localized charge on aspartic acid, the K47D mutation caused intolerable charge repulsion, whereas the longer and more flexible glutamic acid side chain was able to avoid this conflict. Another possible interpretation was that K47D would dramatically lower the intrinsic helicity of that region of the SNARE motif. To address this possibility we created two more mutations; K47N is the most similar possible mutation to K47D with respect to side chain size and shape. K47G tests the inherent susceptibility of the 47^{th} residue to helix disrupting residues. As seen in Fig. 2*B* (*fourth* and *fifth panels*), these mutations reduced SNARE complex formation by 31 and 56%, respectively, indicating that gross helicity affects are unlikely to account for the potency of the K47D mutation. Three additional

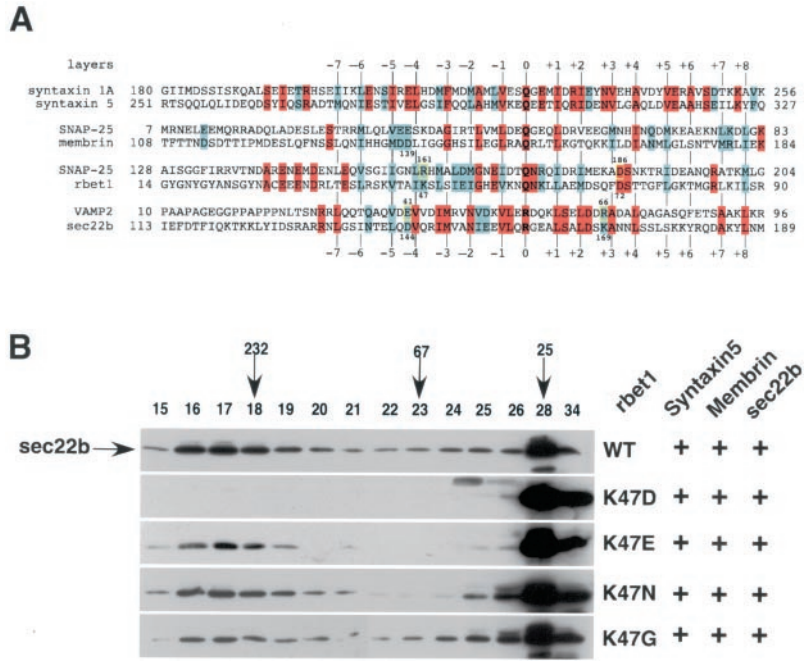

FIG. 2. **A specific charge reversal at a conserved salt bridge eliminates ER/Golgi quaternary complex formation.** *A*, alignments of each ER/Golgi SNARE domain with the most similar SNARE domain from the synaptic complex. Layers of contacting residues on the inner surface of the synaptic complex are numbered *above* and tracked by *vertical lines*. *Bold black residue letters* on sequences highlight the ionic zero layer position. Residue letters colored *red* are identical, and *blue letters* are similar, with the following groupings considered similar: R and K; Q and N; T and S; E and D; and V, I, L, F, and M. Ionic residues that participate in surface salt bridges in the synaptic complex between SNAP-25C and VAMP 2 are highlighted with *yellow*. *B*, ER/Golgi quaternary complex formation as assayed in Fig. 1, except that binding reactions were carried out for 4 h at 4 °C. The only difference between the five reactions is the residue at position 47 of rbet1. Each rbet1 protein was purified with the same procedures and utilized at 2 μM in the binding reactions.

arguments against purely helicity affects are: 1) K47D has a relatively mild effect on rbet1-syntaxin 5 binary interactions (Fig. 3*A*); 2) Specific counter-mutations display mutual complimentarity with rbet1 K47D and can partially rescue the mutation (Fig. 4); and 3) SNARE motifs are inherently adaptable helical domains that have been shown to adapt well to local disruptions in structure (31). In summary, we interpret Fig. 2 to indicate that a likely ionic interaction between rbet1 Lys^{47} and sec22b Asp^{144} contributes significantly to the assembly of the quaternary complex, because all mutations that would lack the ionic interaction are reduced relative to wild type. Our results do not distinguish between effects on kinetics of assembly as opposed to thermal stability of the complex. Secondly, K47D causes an especially dramatic effect perhaps because of localized charge repulsion between the rbet1 and sec22b SNARE motifs. As outlined below, the severity of the mutation probably in part results from repulsions that take place on intermediates in the assembly process rather than simply between the rbet1 47 and sec22b 144 positions.

rbet1 K47D Is Defective at All Levels of Heteromeric SNARE Complex Assembly—If the potent effects of rbet1 K47D on quaternary complex formation (Fig. 2*B*) were simply an effect of charge repulsion between rbet1 and sec22b, then we would not expect the K47D mutation to affect binary and ternary interactions of rbet1. However, as illustrated in Fig. 3*B*, binary interactions between bead-immobilized GST-membrin and soluble rbet1 K47D were severely compromised, with no binary interaction detected until soluble rbet1 concentrations exceeded 2 μM. Interestingly, the other easily detectable binary interaction that rbet1 undergoes in bead binding studies, that between bead-immobilized GST-rbet1 and soluble syntaxin 5 (9), displayed a much more mild defect of the mutation, showing an ~40% reduction in binding in the 0.5–1.5 μM syntaxin 5 concentration range (Fig. 3*A*). Syntaxin 5, membrin, and rbet1 are known to form a stable ternary complex that can be detected easily by bead binding and gel filtration analysis (9). Using bead-immobilized GST-membrin and adding soluble rbet1 to potentiate the binding of soluble syntaxin 5, we found that rbet1 K47D was essentially entirely defective in formation of ternary complexes (Fig. 3*C*). Thus, rbet1 K47D caused a severe disruption in a subset of rbet1 binary interactions as well as rbet1 ternary and quaternary SNARE interactions.

Why would the K47D mutant affect lower order SNARE complex formation? One possibility would be that the lower order complexes have a fundamentally different organization than the quaternary complex and that the aspartate could conflict with another residue besides sec22b Asp^{144}. From the alignment in Fig. 2*A* it is apparent that membrin features an aspartic acid at position 139, which, assuming backbone superimposability, could conflict with K47D if membrin were to occupy the sec22b space in a four-helix bundle. Biophysical studies have demonstrated that most SNARE helical bundles are four-helix bundles, even lower order SNARE complexes that are not sufficient for membrane fusion. For example, the synaptic t-SNARE complex is a parallel four-helix bundle with two copies of syntaxin and one of SNAP-25 (32). In addition, the binary complex between syntaxin 1A and the amino-terminal helix of SNAP-25 is also a four-helix bundle containing two copies of each member (33). Thus, it is not unlikely that the binary and ternary complexes we observe with ER/Golgi Q-SNAREs could have a very different subunit organization from the ER/Golgi quaternary complex.

To test the possibilities that a charge conflict between K47D and sec22b Asp^{144} may be at the heart of the effects on quaternary complex formation and that charge repulsion between rbet1 K47D and membrin Asp^{139} was involved in the effects on lower order complex formation with rbet1 K47D, we created sec22b D144K and membrin D139K mutations and tested these proteins in a series of binding reactions in Fig. 4. For this experiment, binding reactions were analyzed by gel filtration, and rbet1, rather than sec22b, was used as the tracer to indicate complex formation. We quantified only the high molecular mass gel filtration fractions rather than analyzing each entire gel filtration profile. As shown in Fig. 4*A*, a strong high molecular mass rbet1 signal is produced by binary, ternary, and quaternary binding reactions using wild type rbet1. Note that a limitation of this experiment is that we cannot distinguish, for example in the quaternary mixture, how much of the high molecular mass rbet1 is present as a quaternary complex as opposed to ternary and binary species. However, no rbet1 signal is detected when rbet1 alone is analyzed or in a binary mixture between rbet1 and membrin D139K, indicating that membrin D139K is completely nonfunctional for binding to wild type rbet1. We then examined a variety of binding reac-

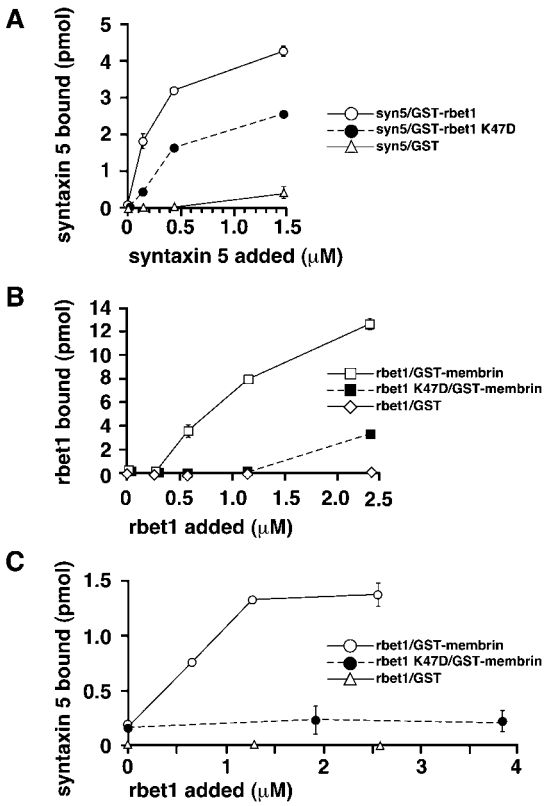

FIG. 3. **rbet1 K47D is defective for binary and ternary SNARE interactions.** *A*, binary bead binding reactions testing syntaxin 5 binding to GST-rbet1 beads (*syn5/GST-rbet1*), syntaxin 5 binding to GST-rbet1 K47D beads (*syn5/GST-rbet1 K47D*), or syntaxin 5 binding to GST beads (*syn5/GST*). *B*, binary bead binding reactions testing rbet1 binding to GST-membrin beads (*rbet1/GST-membrin*), rbet1 K47D binding to GST-membrin beads (*rbet1 K47D/GST-membrin*), and rbet1 binding to GST beads (*rbet1/GST*). *C*, ternary bead binding reactions testing syntaxin 5 binding to GST-membrin beads in the presence of varying concentrations of rbet1 (*rbet1/GST-membrin*), syntaxin 5 binding to GST-membrin beads in the presence of varying concentrations of rbet1 K47D (*rbet1 K47D/GST-membrin*), or syntaxin 5 binding to GST beads in the presence of varying concentrations of rbet1 (*rbet1/GST*).

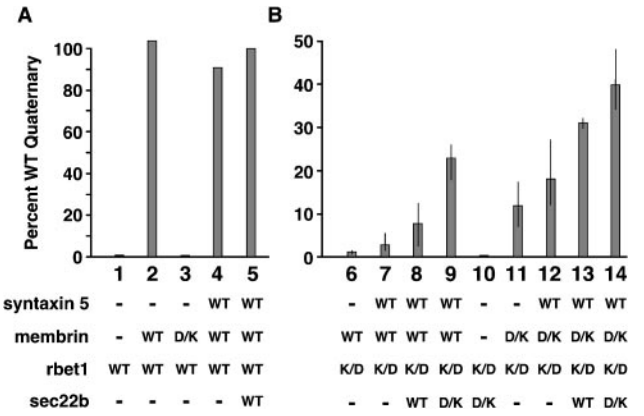

FIG. 4. **Charge reversal mutations on sec22b and membrin partially restore SNARE complex assembly with rbet1 K47D.** Purified, bacterially produced recombinant SNAREs were mixed in the combinations indicated below and incubated 2 h at 4 °C. Each protein had a final concentration of ~2 μM and was used at an identical concentration in every reaction. For analysis, the binding reactions were gel-filtered on Superdex 200, and a pool of fractions 16–18 was immunoblotted for the presence of rbet1 and quantitated. The rbet1 signal in each condition was normalized to that in condition 5. *A*, binding reactions employing wild type rbet1. The values plotted are representative single determinations. *B*, binding reactions employing rbet1 K47D. The values plotted are the means of three independent determinations, with the range of values indicated. *WT*, wild type; *K/D*, rbet K47D; D/K, membrin D139K (conditions 3 and 11–14) and sec 22b D144K (conditions 9, 10, and 14).

tions utilizing rbet1 K47D and tested the ability of membrin D139K and sec22b D144K to rescue the different levels of complex formation. As shown in Fig. 4*B*, binary, ternary, and quaternary SNARE interactions with wild type membrin and sec22b resulted in little high molecular mass rbet1 K47D signal (*lanes 6–8*), consistent with the experiments in Figs. 2 and 3. However, membrin D139K was able to partially restore a significant signal in binary and ternary incubations with rbet1 K47D (*lane 6 versus lane 11* and *lane 7 versus lane 12*). These results demonstrate mutual complementarity between rbet1 K47D and membrin D139K (*lanes 3* and *6 versus lane 11*) and are consistent with a conflict between rbet1 K47D and membrin Asp^{139} being at least partially responsible for the unexpected effects of that mutation on lower order complexes. This is also consistent with our suggestion that in binary and ternary complexes, membrin might occupy a position similar to that of VAMP in the synaptic complex. One possibility is that in these complexes, there are two copies of membrin, one in the Q_B position and another in the R position. Unexpectedly, it also appeared that membrin D139K contributed to quaternary complex formation (*lane 12 versus lane 13*); however, the rbet1 signal in *lane 13* is presumably a mixture of binary, ternary, and quaternary complexes, making it difficult to isolate the effects on the different complexes. On the other hand, as shown in *lane 8 versus lane 9*, sec22b D144K partially rescued quaternary complex formation. Because the only sec22b interactions detectable by gel filtration are quaternary (9) (also true for yeast Sec22p in Fig. 1*D* of this manuscript), it is safe in this case to assume that most of the rbet1 signal in *lane 9* represents quaternary complexes. Rescue of quaternary complex by sec22b D144K was also detectable using sec22b as the tracer in gel filtration (data not shown). In conclusion, membrin D139K partially restores lower order complex formation to rbet1 K47D, consistent with membrin occupying the R position in those complexes, and sec22b D144K partially restores quaternary complex formation to rbet1 K47D, consistent with sec22b occupying the R position in that complex. The finding that membrin D139K may restore some quaternary complex to rbet1 K47D could indicate that lower order complexes may nucleate or facilitate formation of the quaternary complex. Because we used relatively short incubation times for these experiments, we cannot distinguish effects of the different mutations on the kinetics of assembly from effects on the thermodynamic stability of the final product. *Lane 14* illustrates that the combination of membrin D139K and sec22b D144K restores quaternary complex formation to rbet1 K47D by over 40%. All of the effects of the mutations we examined are consistent with our hypothesis about the arrangement of the ER/Golgi quaternary complex and inconsistent with the proposal that rbet1 plays the canonical v-SNARE role in that complex.

Determinants for rbet1 SNARE Interactions and Vesicle Coat Interactions Differ in Vivo—The yeast Bet1p SNARE motif is required for its interactions with both the COPII and COPI coat systems (24, 25). The dramatic effects of the rbet1 K47D mutation gave us the opportunity to examine the relationship between rbet1 SNARE interactions and other protein interactions in which the SNARE motif participates. To examine the effects of the K47D mutation on various protein interactions, we transfected NRK cells with either wild type Myc-rbet1 or Myc-rbet1 K47D and then performed immunoprecipitation experiments from detergent extracts of the cells. As shown in Fig. 5, syntaxin 5 immunoprecipitation resulted in membrin coprecipitation in either lysate but only Myc-rbet1 wild type

co-precipitated with syntaxin 5 to a significant extent. Interactions between syntaxin 5 and Myc-rbet1 K47D were reduced by 91% relative to wild type. Because Myc-rbet1 and Myc-rbet1 K47D were expressed at equivalent levels, this indicated that the K47D mutation was equally disruptive of SNARE interactions *in vivo* as it was *in vitro* with recombinant proteins. In reciprocal immunoprecipitations with anti-Myc antibodies, syntaxin 5 was efficiently immunoprecipitated in the Myc-rbet1 lysates and reduced by 93% in the Myc-rbet1 K47D lysate, again consistent with the dramatic effects of this mutation in *in vitro* binding studies. In stark contrast, immunoprecipitations with anti-β-COP antiserum resulted in equal co-immunoprecipitation of both Myc-rbet1 constructs. Our interpretation of this result was that the interaction between the rbet1 SNARE motif and the COPI machinery is entirely independent of heteromeric SNARE interactions. Whatever structural properties of the SNARE motif are required for COPI interactions are completely preserved in the K47D construct that is largely incapable of participating in ER/Golgi SNARE bundles.

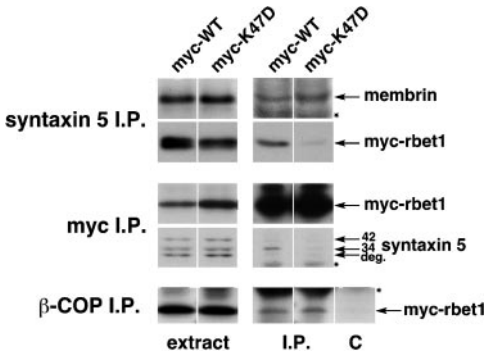

FIG. 5. **rbet1 K47D exhibits dramatically reduced SNARE interactions but unaffected coatomer interactions *in vivo*.** NRK cells were transfected with either wild type Myc-rbet1 (*myc-WT*) or Myc-rbet1 K47D (*myc-K47D*). Whole cell Triton X-100 lysates were prepared, subjected to immunoprecipitation (*I.P.*) with the antisera shown on the *left*, and subjected to immunoblotting with the antisera indicated on the *right*. The columns marked *extract* represent 1% of the extract subjected to immunoprecipitation and displayed in the columns labeled *I.P.* The three immunoprecipitations were carried out in three different transfection experiments. The *box* labeled *C* was a mock immunoprecipitation carried out with protein A beads lacking primary antibody. *Asterisks* denote the positions of antibody light chains.

rbet1 SNARE Interactions and Proper Intracellular Targeting Are Independent Functions of the SNARE Motif—An important question that has not been resolved involves the relationship between SNARE interactions and SNARE targeting in the secretory pathway. For example, does a t-SNARE complex get targeted to its vesicles of function, or does it form there from individually trafficked SNAREs? Because rbet1 appeared to play the role of Q_C-SNARE in a putative t-SNARE complex, because rbet1 is known to undergo rapid constitutive cycling between the ER and Golgi, and because we had powerful and specific mutations that affected its ability to form SNARE complexes, we had a good opportunity to examine whether SNARE interactions are important for any aspect of proper rbet1 targeting. First, we wanted to establish whether the rbet1 SNARE motif itself was even important for rbet1 targeting. As demonstrated in Fig. 6A in the *top row*, expression of Myc-rbet1 in NRK cells resulted in a juxtanuclear, Golgi-like concentration of staining similar to the *cis*-Golgi marker GM130 but with a significant number of peripheral spots representing VTCs and/or ER exit sites (23, 34). This distribution of recombinant protein was similar to the endogenous rbet1 (Fig. 6*A*, *third row*), except that the balance between Golgi area staining and peripheral spots is noticeably shifted toward Golgi in the recombinant case, perhaps because of higher expression levels. On the other hand, when the rbet1 cytoplasmic domain was removed and replaced with GFP, the hybrid construct, GFP-rbet1TM, did not localize properly. As shown in Fig. 6*B* (*left panel*), GFP-rbet1TM was mislocalized primarily to ER tubules, demonstrating that unlike syntaxin 5 and several others, the rbet1 transmembrane domain is not sufficient for

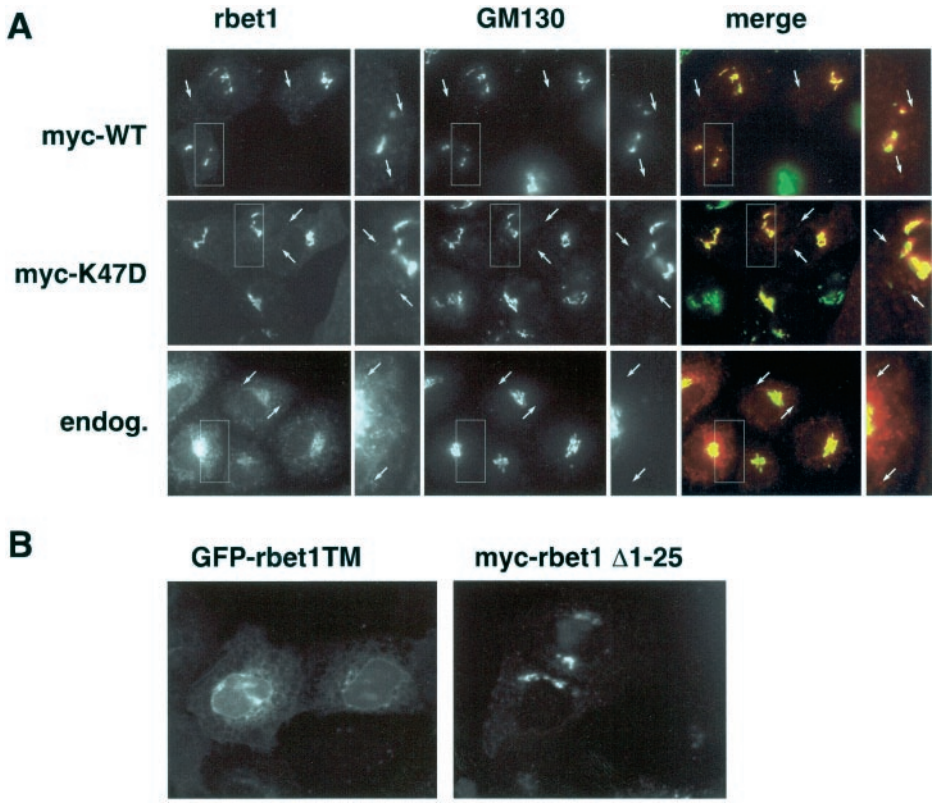

FIG. 6. **The SNARE motif of rbet1 directs proper steady-state localization independently of SNARE interactions.** *A*, the *top two rows* show immunofluorescence images of NRK cells transfected with wild type Myc-rbet1 (*myc-WT*) or Myc-rbet1 K47D (*myc-K47D*) stained with anti-Myc (*red*) or GM130 (*green*) antibody. Individual *red* and *green* stainings are shown as grayscale as well as the colored merge. The areas inside *white boxes* are expanded to the *right* of each larger panel for greater detail. The *arrows* indicate peripheral staining exhibited by rbet1 constructs but not by GM130. The *third row* shows the same features of endogenous (*endog.*) rbet1 staining in nontransfected NRK cells. *B*, steady-state localization of the indicated constructs in transfected NRK cells.

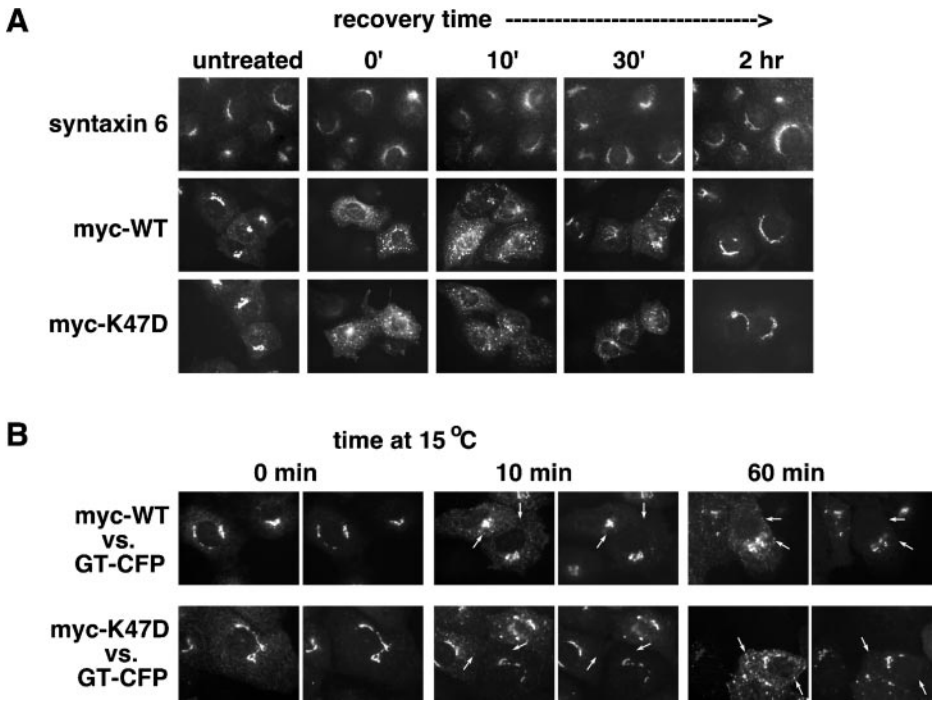

FIG. 7. **The intracellular dynamics and constitutive recycling of rbet1 are independent of SNARE interactions.** *A*, NRK cells were transfected with wild type Myc-rbet1 (*myc-WT*) or Myc-rbet1 K47D (*myc-K47D*) and subjected to a 1-h brefeldin A treatment. Brefeldin A was removed, and the cells were allowed to recover for the indicated lengths of time prior to fixation and staining with anti-Myc (*bottom two rows*) or anti-syntaxin 6 (*top row*) antibodies. The *left column* illustrates steady-state staining prior to BFA addition. *B*, NRK cells were co-transfected with either wild type Myc-rbet1 (*myc-WT*) or Myc-rbet1 K47D (*myc-K47D*) and the localization domain of galactosyltransferase linked to CFP (*GT-CFP*). The cells were shifted from 37 to 15 °C and incubated for 0, 10, or 60 min prior to fixation and staining with anti-Myc antibody. For each time point, a pair of images are displayed showing anti-Myc (*left*) and CFP (*right*) fluorescence. The peripheral rbet1 staining became progressively more intense relative to rbet1 juxtanuclear staining and CFP fluorescence and the peripheral spots became larger with increased time at 15 °C (examples are marked by *arrows*).

proper targeting and that essential targeting information resides in the cytoplasmic domain. Unlike many SNAREs, rbet1 lacks an independent amino-terminal domain and contains only an ~25 residue amino-terminal peptide prior to the SNARE motif. Removal of the first 25 amino acids of the rbet1 cytoplasmic domain did not significantly perturb rbet1 localization (Fig. 6*B*, *right panel*), indicating that like syntaxin 6, another Q_C-SNARE with a cyclical itinerary, essential targeting determinants reside within the SNARE motif itself (18, 19).

We next compared the subcellular distributions of wild type Myc-rbet1 and Myc-rbet1 K47D in transfected NRK cells. As seen in Fig. 6*A* (*top two rows*), the steady-state distribution of the mutant was indistinguishable from the wild type construct, indicating that SNARE interactions do not influence steady-state targeting of rbet1. However, we also wanted to determine whether, like endogenous rbet1, the mutant construct was able to engage in identical dynamics and constitutive cycling between the ER and Golgi. We investigated the dynamics of the recombinant constructs using experimental perturbations that preferentially affect one leg of the recycling pathway. As shown in Fig. 7*A* (*second* and *third rows*), extensive brefeldin A treatment of NRK cells resulted in dispersion of both Myc-rbet1 constructs into large, punctate, "frustrated" ER exit sites or VTCs (35–37). This is in contrast to typical Golgi resident proteins, which are diluted into a fine, reticular, ER pattern by this treatment (not shown), and *trans*-Golgi network proteins, such as syntaxin 6 (Fig. 6*A*, *top row*), which are barely affected by BFA. The concentration of the rbet1 constructs in the ER exit structures is indicative of strong determinants for a cyclical vesicle localization, as opposed to a static localization. When brefeldin A was removed from the cells, both constructs transitioned with equal time courses out of ER exit sites to the central juxtanuclear localization seen at steady state. We interpret the BFA results to indicate that heteromeric SNARE interactions have no impact on the strong forward recruitment of rbet1 from the ER to Golgi. We also incubated transfected NRK cells at 15 °C, a treatment known to trap rapidly recycling proteins in newly formed peripheral VTCs (38). We used the rate of redistribution from the Golgi area to peripheral VTCs as an indication of rbet1 recycling rate in the early secretory pathway. As seen in Fig. 7*B* (*left panel* of each pair), both wild type Myc-rbet1 and Myc-rbet1 K47D peripheral staining began to intensify after as little as 10 min at 15 °C and was further dispersed after 60 min. To demonstrate specificity, we co-transfected the cell with a CFP-tagged galactosyltransferase construct that localizes to Golgi stacks and did not redistribute significantly over this time course (Fig. 7*B*, *right panel* of each pair). In summary, from the experiments of Figs. 6 and 7, we conclude that rbet1 SNARE interactions are entirely dispensable to rbet1 steady-state targeting or dynamic cycling in the early secretory pathway. Although we cannot eliminate the possibility that SNARE complexes containing rbet1 are trafficked along this itinerary under the wild type condition, it does appear that heteromeric SNARE bundles are not a required or strongly favored mode of rbet1 targeting.

SNARE Interactions Are Dispensable for rbet1 Recruitment onto Budding Transport Vesicles—A recent study reported that ARF-GAP induced a conformational change in the Bet1p SNARE motif that primed this domain for direct interactions with the COPI and even the COPII coat machinery (25). Although the nature of the conformational change was not investigated, one suggestion was that it may be the induction of SNARE bundling that increased its affinity for the coats. Furthermore, it was suggested that priming of SNARE motifs by ARF-GAP may be essential for recruitment of the SNAREs into transport vesicles. Because the Myc-rbet1 K47D mutant is defective for SNARE interactions, we asked whether the lack of SNARE interactions influenced the efficiency of recruitment of this SNARE onto coated vesicles. We developed a simple coated vesicle generation assay that employs scrape-permeabilized NRK cells as a source of donor ER and Golgi. No attempt is made to separate nor discriminate in this assay between recruitment to COPI and COPII vesicles. As seen in Fig. 8*A*, after incubation of the washed permeabilized cells with cytosol and an ATP-regenerating system followed by pelleting of the cells, the supernatant contained slowly sedimenting membranes that could be resolved by floatation on an Optiprep gradient. Coated transport vesicles appeared to migrate to fractions 7 and 8 on the Optiprep gradients, as indicated by the convergence of COPI, COPII, SNAREs, and the cycling vesicle constituent p24 in those fractions. A less dense peak of SNAREs appeared in fractions 3 and 4 but did not co-fractionate with

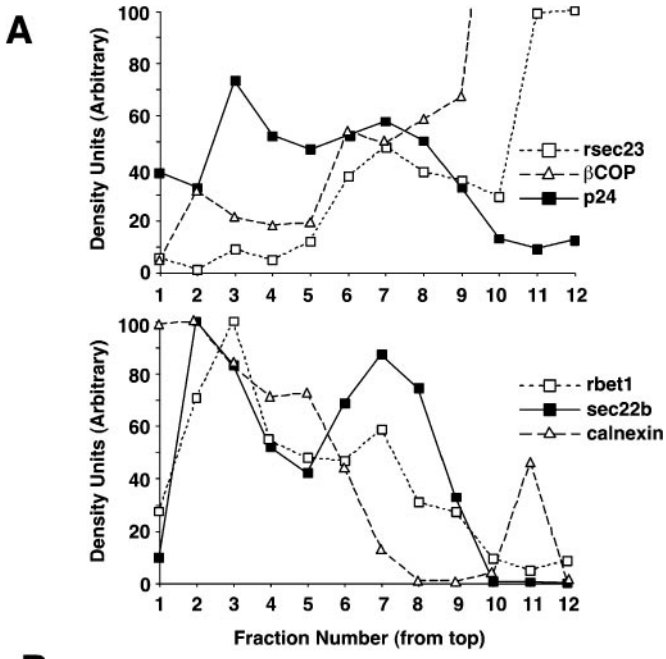

FIG. 8. **Efficient recruitment of rbet1 onto transport vesicles is independent of SNARE interactions.** *A*, equilibrium density gradient analysis of diffusible vesicles released from permeabilized cells in the presence of cytosol and ATP at 32 °C. The permeabilized cells were incubated as detailed under "Experimental Procedures," and diffusible vesicles were isolated by differential centrifugation followed by floatation into continuous iodixanol gradients. The fractions were unloaded from the top and analyzed by immunoblotting and quantitation of the indicated proteins. *B*, rbet1 K47D budding requirements and efficiency are indistinguishable from wild type (*WT*). NRK cells were transfected with wild type Myc-rbet1 or Myc-rbet1 K47D, permeabilized, and subjected to budding reactions with or without MgATP, cytosol, or elevated temperature as indicated. The coated vesicle population was isolated by differential centrifugation and floatation in iodixanol gradients as in *A*. Fractions from the peak of coated vesicles (fractions 6–8) were immunoblotted for the proteins listed on the *left*. The *right column* shows 2% of each protein in the starting permeabilized cells as an indication of relative budding efficiency. *rbet1* refers to endogenous rbet1 detected with anti-rbet1 antisera, whereas the Myc constructs were detected with anti-Myc antibodies.

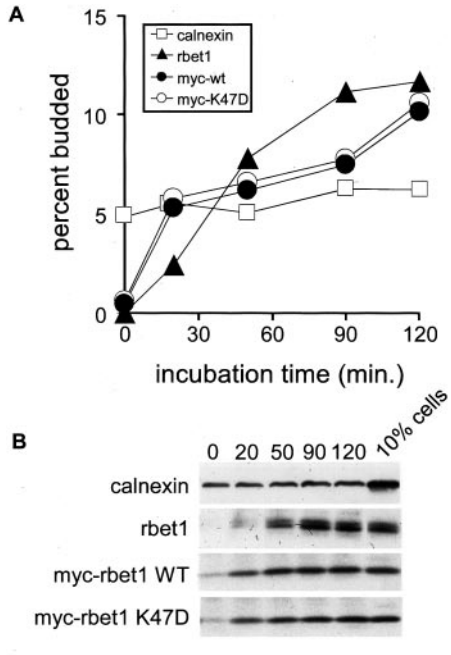

FIG. 9. **Disruption of SNARE interactions does not affect the rate of rbet1 incorporation into coated vesicles.** NRK cells were transfected with either wild type Myc-rbet1 or Myc-rbet1 K47D, permeabilized and subjected to budding reactions containing cytosol and MgATP for the indicated times at 32 °C. Released diffusible vesicles were then isolated by differential centrifugation and immunoblotted for the presence of the indicated proteins. *A* shows quantitation of the immunoblots, which are shown in *B*. The *right column* in *B* shows the amount of each protein in 10% of the starting permeabilized cells. This quantity was used to calculate the percentage of budding efficiency plotted on the *y* axis in *A*. *WT* and *wt*, wild type.

coat subunits. The relative size of this less dense peak varied considerably between experiments, whereas the putative coated vesicle peak remained stable. Although we have not identified the less dense membranes, we speculate that they may represent uncoated vesicles, VTCs, or a fusion product of vesicles from the incubation. These early fractions were not well separated from apparently nonspecific ER fragments containing calnexin that were released without regard to temperature, cytosol, or energy. In the experiment in Fig. 8*B*, we used the Optiprep gradients to isolate the coated vesicle fraction following budding incubations and examined the biochemical requirements for budding and the vesicle recruitment efficiencies of different proteins. The coated vesicle fraction from budding reactions contained the expected array of ER/Golgi SNAREs (syntaxin 5, membrin, rbet1, and sec22b), vesicle machinery (p24, COPI, and COPII coat subunits βCOP and rsec13, respectively), and cargo (not shown; vesicular stomatitus virus G protein), in a temperature-, cytosol-, and nucleotide-dependent fashion. On the other hand, ER resident proteins (protein disulfide isomerase, calnexin, and glucosidase) that were abundant in the permeabilized cells were specifically de-enriched in the vesicle fraction. We found that SNAREs, especially sec22b, were very efficiently incorporated into these vesicles. Interestingly, rbet1 and membrin recruitment was efficient but less energy-dependent than other vesicle constituents (Fig. 8*B*, *second* and *fourth rows versus first*, *third*, *eighth*, and *ninth rows*). This may have to do with the observation in yeast that Bet1p and Bos1p seem to interact most strongly with the coat machinery (24). In fact, ARF-GAP was able to induce interactions between these SNAREs and both coats even in the absence of the GTPases Arf1p and Sar1p (25). Hence, it is conceivable that in the absence of nucleotides, membrin and rbet1 are packaged at a reduced efficiency into artifactual vesicles that lack other SNAREs, vesicle machinery, and cargo.

Importantly, both transfected wild type Myc-rbet1 and Myc-rbet1 K47D were packaged into diffusible transport vesicles with the same biochemical requirements and overall efficiency (Fig. 8*B*, *fifth* and *sixth rows*). Because we wanted to determine whether SNARE interactions were required for optimal packaging, we also examined the time course of recruitment/budding of the Myc-rbet1 constructs relative to each other and

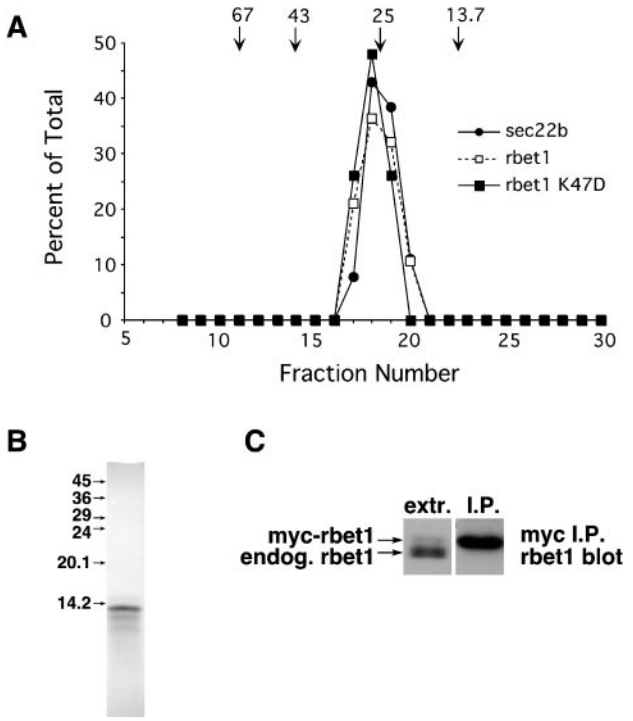

FIG. 10. **rbet1 does not engage in stable self-associations *in vitro* or *in vivo*.** *A*, gel filtration analysis of purified rbet1 and sec22b cytoplasmic domains on Superdex 75. Elution positions of globular markers are indicated above. *B*, SDS-PAGE of the rbet1 preparation employed for analytical ultracentrifugation, stained with Coomassie Blue. *C*, immunoprecipitation (*I.P.*) of wild type Myc-rbet1 from NRK cell detergent extracts did not co-precipitate endogenous rbet1. NRK cells were transfected with wild type Myc-rbet1, subjected to Triton X-100 extraction, and immunoprecipitated with anti-Myc antisera. Immunoblotting was carried out with anti-rbet1 antisera that recognizes both endogenous (*endog.*) rbet1 and transfected Myc-rbet1.

relative to endogenous rbet1. As shown in Fig. 9, both constructs exhibited very similar time courses of budding, reaching a value of about 10% incorporation of the total cellular pool by 90 min of incubation, as did the endogenous rbet1. Our interpretation of these results is that rbet1 SNARE interactions are largely dispensable for recruitment to transport vesicles in the early secretory pathway. It seems likely that interactions between the SNARE motif and the coat machinery are at least partly responsible for recruitment into vesicles and by extension that these interactions involve conformations/structural determinants that are independent of the SNARE binding determinants.

Evidence against rbet1 Homo-oligomeric SNARE Bundles—Our data indicate that heteromeric SNARE interactions, *e.g.* involving t-SNARE complexes, are not essential for rbet1 targeting or recruitment to vesicles. However, it does not necessarily address whether homo-oligomeric SNARE interactions play an essential role. Some SNAREs apparently form homodimers *in vitro* and/or *in vivo*, and these interactions may involve distinct determinants from heteromeric SNARE interactions (39). Yeast Bet1p homo-oligomerization was suggested as a possible ARF-GAP-induced trigger for SNARE-coat interactions (25). We were thus interested in whether homomeric interactions of the rbet1 SNARE motif occur and could be important for its targeting function. We first investigated the oligomeric state of purified rbet1 using gel filtration on Superdex 75. rbet1 cytoplasmic domain eluted with a calculated molecular mass of ~25 kDa (Fig. 10*A*). rbet1 K47D cytoplasmic domain behaved similarly (Fig. 10*A*). The rbet1 constructs employed in these studies had a calculated monomer molecular mass of ~11 kDa, significantly less than their elution volume

TABLE I
Single species analysis of sedimentation equilibrium data for rbet1 cytoplasmic domain

Speed	Molecular mass
	Da
30,000	10,340 ± 1,470
35,000	10,190 ± 1,100
40,000	9,530 ± 1,160
Global	9,830 ± 950

suggested and approximately half the size of the sec22b cytoplasmic domain, despite the fact that rbet1 and sec22b coeluted. Because this rbet1 gel filtration behavior was consistent with a stable rbet1 dimer, we performed AU on isolated wild type rbet1 cytoplasmic domain to rigorously determine its oligomeric state. The calculated molecular mass of our rbet1 construct based upon amino acid composition is 11,072 Da. Single species analysis provides an apparent molecular mass of 9,830 ± 950 Da (Table I). Although this molecular mass is lower than that expected for a monomer, if we take account of the presence and abundance of rbet1 degradation products present in our AU preparation (Fig. 10*B*), the calculated average theoretical molecular mass drops to 10,632 Da, which is then in good agreement with that determined by AU. There appears to be a small speed dependence in the molecular masses (Table I), which is consistent with the heterogeneity in the sample (Fig. 10*B*). In summary, the AU analysis indicates that the rbet1 SNARE motif is essentially monomeric and that the unexpectedly small gel filtration volume must be due to unusual properties of rbet1 rather than homo-oligomerization. Although the AU was carried out with relatively dilute protein (1 μM), gel filtrations over a range of concentrations indicated that the oligomeric state of rbet1 was stable up to 10 μM. We speculate that the aberrant gel filtration volume may be due to the rbet1 SNARE motif existing in an unstructured, nonglobular state. Several SNARE motifs have been shown to be unstructured when unbound (31, 40).

To test whether rbet1 forms homo-oligomers *in vivo*, we investigated whether interactions between wild type Myc-rbet1 and endogenous untagged rbet1 were detectable in cell lysates. As shown in Fig. 10*C*, efficient immunoprecipitation of Myc-rbet1 from NRK cell extracts did not result in detectable co-precipitation of endogenous rbet1, using the same conditions in which heteromeric interactions with syntaxin 5 were easily detectable (Fig. 5). In summary, although we cannot rule out low level or transient homo-oligomeric SNARE interactions contributing to rbet1 targeting and vesicle recruitment, our data do not support a role for rbet1 homo-oligomers as a significant species in cells. Instead, our data are most consistent with the targeting machinery operating independently of SNARE interactions altogether. Further studies will be needed to delineate the structural features of the SNARE motif required for rbet1 targeting.

DISCUSSION

How Is the ER/Golgi SNARE Complex Organized?—Our biochemical substitution experiments (Fig. 1) and interchain interaction data (Figs. 2–4) support a conserved organization of the ER/Golgi complex relative to the synaptic and endosomal four-helix bundles, with membrin and rbet1 playing roles analogous to those of SNAP-25N and SNAP-25C, respectively, and sec22b corresponding spatially to VAMP 2. Thus, the simplest interpretation of our data would be that *in vivo* sec22b opposes a t-SNARE complex comprised of syntaxin 5, membrin, and rbet1. In further support of this model, sec22b appears to bind strongly only to the combination of all three Q-SNAREs, making its binding a logical membrane-bridging step (9). How can

we reconcile our data with the well established fact that this expected topology does not support liposome fusion *in vitro* (13)? Reconciliation may not actually be necessary, because the lack of fusion with opposing sec22b is actually *predicted* from our data. An unexpected feature of the ER/Golgi SNAREs is that syntaxin 5, membrin, and rbet1 form a kinetically trapped SNARE complex that cannot accept a molecule of sec22b and thus cannot advance to form a quaternary complex (9). *In vitro*, the quaternary complex forms only when all four proteins are added simultaneously. The unexpected topology found to mediate liposome fusion, with Sed5p (syntaxin 5), Bos1p (membrin), and Sec22p on one membrane is unique in that this combination of SNAREs do not interact significantly and would thus "postpone" SNARE complex formation until all four SNAREs came together simultaneously in the presumed docking event. The important issue is whether the kinetically trapped SNARE complex is in fact an *in vitro* artifact because of the lack of SNARE regulatory factors. If, *in vivo*, other factors prevent formation of or otherwise remediate this presumably off-pathway intermediate, then membrane fusion could conceivably proceed via the conserved topology at least as rapidly as in any other topology. Consistent with this, Sec22p did catalyze liposome fusion in the v-SNARE topology when opposed to the functional t-SNARE comprised of Sso1p and Sec9p (3). A direct test of this hypothesis would require identification of the presumed factors that regulate ER/Golgi t-SNARE assembly and activity.

If, on the other hand, ER/Golgi SNARE complex formation *in vivo* proceeds in the nonconserved topology suggested by liposome fusion studies, then how could we interpret our substitution data? One possibility is that the SNARE motif positions in the complex are conserved, as suggested by the substitutions and by the crystal structure of the endosomal complex (7), but that membrane topology is not. That is, perhaps rbet1 could in fact be a SNAP-25C homolog and hold that position in the complex and at the same time be anchored in the opposite membrane from syntaxin 5, membrin, and sec22b. This would represent a functional dissociation of the SNARE complex structure from the topology of the proteins and could have important consequences for the intermediate steps and route of SNARE complex assembly. Further work in more physiological contexts will be required to determine whether this kind of flexibility exists *in vivo*.

The mechanistic basis of the kinetically trapped ternary complex has not been investigated. However, new data in this manuscript suggest that the syntaxin 5-membrin-rbet1 complex contains a membrin aspartate 139 in contact with rbet1 lysine 47. In other words, this ternary complex most likely contains a membrin molecule positioned like VAMP or sec22b. This membrin molecule could prevent entry of sec22b and quaternary complex formation, thus potentially explaining the "locked" t-SNARE phenomenon (9). This could either represent a "misplaced" membrin molecule in a 1:1:1 ternary complex or an "extra" copy of membrin in a 1:1:2 ternary complex. We previously reported a 1:1:1 subunit stoichiometry of the ternary complex (9) after isolation of this complex using an anti-rbet1 monoclonal antibody. We were unable to produce sufficiently pure quantities of the ternary complex for a stoichiometric analysis without immunoprecipitation. It is possible that the rbet1 immunoprecipitation affected the stoichiometry and that the 1:1:1 stoichiometry we obtained was incorrect. Greater quantities of purified complex will be required for a more precise analysis.

The rbet1 SNARE Motif Mediates Proper rbet1 Targeting and Dynamic Cycling in the Absence of Heteromeric SNARE Interactions—Unlike syntaxins 3, 4, and 5, whose transmembrane domains were reported to be sufficient to specify their steady-state localizations (14–16), rbet1 requires its SNARE motif for proper targeting (Fig. 6). This finding is reminiscent of the *trans*-Golgi network/endosomal SNARE syntaxin 6, which is actually not a syntaxin but a Q_C-SNARE, like rbet1 (19). Because the SNARE motif plays a required role in targeting, one wonders whether its interactions with other SNAREs, *e.g.* syntaxin 5 and membrin, could be key determinants in this process. However, our data clearly refute this conjecture and demonstrate that the rbet1 SNARE motif can specify all aspects of the dynamic targeting of rbet1 independently of SNARE complexes. Thus, targeting appears to represent a truly autonomous function of the rbet1 SNARE motif. This does not rule out the possibility that t-SNARE complexes are trafficked between the ER and Golgi but does rule out the possibility that they are a favored substrate of the targeting machinery. We also cannot rule out that other SNAREs are dependent upon SNARE interactions with rbet1 for their proper localizations. It is also formally possible that very low levels or transient SNARE interactions that persist in the rbet1 K47D mutant play an essential role, although reduced by 92% relative to wild type (Fig. 5).

What protein interactions are required for dynamic rbet1 targeting? The best candidate interactions are between the rbet1 SNARE motif and the coat machinery. Although we cannot rule out interactions with other types of proteins, strong interactions with both coat systems could conceivably be sufficient to impart rbet1 with constitutive cycling and proper steady-state localization. Direct interactions between the Bet1p SNARE motif and COPII (24) as well as COPI (25) subunits have been documented, although the precise structural determinants required and their relationship to SNARE complex assembly are unknown. Interestingly, ARF-GAP primed SNAREs for binding to both coat systems (25), possibly indicating a conserved mode of interaction with both coats and similar conformational requirements. One suggestion was that ARF-GAP may prepare Bet1p for coat interactions by inducing SNARE bundling (25). Our results argue strongly against heteromeric SNARE bundling as the prevalent mode of interactions with the vesicle machinery *in vivo*, because rbet1 K47D was efficiently recruited and packaged (Figs. 8 and 9). Although homodimeric bundling of Bet1p could have been the ARF-GAP-dependent event in the previous study, we did not find evidence of a prevalent rbet1 homo-oligomer in solution or in detergent extracts of cells (Fig. 10). Although rbet1 lacks a significant amino-terminal domain, yeast Bet1p contains a 52-amino acid amino-terminal extension that, according to the PSIPRED algorithm (19), contains at least one significant length of α-helix. One possibility is that ARF-GAP primed Bet1p for coat interactions not by bundling the SNARE motif but by altering a potential interaction between the amino-terminal extension and the SNARE motif. This type of regulation might not be relevant to rbet1, which lacks a significant amino-terminal extension.

Because SNARE bundles were not required for rbet1 targeting and because the rbet1 SNARE motif may be unstructured on its own, one possibility is that the coat machinery binds the rbet1 SNARE motif in a fully extended conformation. This would be reminiscent of the binding of botulinum toxin B to the extended VAMP 2 SNARE motif (41). If the targeting machinery does in fact bind to rbet1 in an extended conformation, then only nonbundled SNARE motifs would be included, and the active trafficking of SNARE complexes would be prohibited. Although we did not observe an increase in the rate of trafficking or recruitment to vesicles of rbet1 K47D relative to wild type rbet1, it

is possible that the half-life of rbet1 SNARE complexes *in vivo* is too short to cause a noticeable lag in trafficking.

Acknowledgment—We are indebted to Dr. Fred Hughson (Princeton) for very helpful discussions.

REFERENCES

1. Sollner, T., Whiteheart, S. W., Brunner, M., Erdjument-Bromage, H., Geromanos, S., Tempst, P., and Rothman, J. E. (1993) *Nature* **362,** 318–324
2. Hay, J. C. (2001) *Exp. Cell Res.* **271,** 10–21
3. McNew, J. A., Parlati, F., Fukuda, R., Johnston, R. J., Paz, K., Paumet, F., Sollner, T. H., and Rothman, J. E. (2000) *Nature* **407,** 153–159
4. Wang, Y., Dulubova, I., Rizo, J., and Sudhof, T. C. (2001) *J. Biol. Chem.* **276,** 28598–28605
5. Sutton, R. B., Fasshauer, D., Jahn, R., and Brunger, A. T. (1998) *Nature* **395,** 347–353
6. Antonin, W., Holroyd, C., Fasshauer, D., Pabst, S., Von Mollard, G. F., and Jahn, R. (2000) *EMBO J.* **19,** 6453–6464
7. Antonin, W., Fasshauer, D., Becker, S., Jahn, R., and Schneider, T. R. (2002) *Nat Struct Biol* **14,** 14
8. Fukuda, R., McNew, J. A., Weber, T., Parlati, F., Engel, T., Nickel, W., Rothman, J. E., and Sollner, T. H. (2000) *Nature* **407,** 198–202
9. Xu, D., Joglekar, A. P., Williams, A. L., and Hay, J. C. (2000) *J. Biol. Chem.* **275,** 39631–39639
10. Fasshauer, D., Sutton, R. B., Brunger, A. T., and Jahn, R. (1998) *Proc. Natl. Acad. Sci. U. S. A.* **95,** 15781–15786
11. Bock, J. B., Matern, H. T., Peden, A. A., and Scheller, R. H. (2001) *Nature* **409,** 839–841
12. Weimbs, T., Mostov, K., Low, S. H., and Hofmann, K. (1998) *Trends Cell Biol.* **8,** 260–262
13. Parlati, F., McNew, J. A., Fukuda, R., Miller, R., Sollner, T. H., and Rothman, J. E. (2000) *Nature* **407,** 194–198
14. Banfield, D. K., Lewis, M. J., Rabouille, C., Warren, G., and Pelham, H. R. (1994) *J. Cell Biol.* **127,** 357–371
15. Watson, R. T., and Pessin, J. E. (2001) *Am. J. Physiol.* **281,** C215–C223
16. Kasai, K., and Akagawa, K. (2001) *J. Cell Sci.* **114,** 3115–3124
17. Bock, J. B., Klumperman, J., Davanger, S., and Scheller, R. H. (1997) *Mol. Biol. Cell* **8,** 1261–1271
18. Watson, R. T., and Pessin, J. E. (2000) *J. Biol. Chem.* **275,** 1261–1268
19. Misura, K. M., Bock, J. B., Gonzalez, L. C., Jr., Scheller, R. H., and Weis, W. I. (2002) *Proc. Natl. Acad. Sci. U. S. A.* **99,** 9184–9189
20. Grote, E., Hao, J. C., Bennett, M. K., and Kelly, R. B. (1995) *Cell* **81,** 581–589
21. Hao, J. C., Salem, N., Peng, X. R., Kelly, R. B., and Bennett, M. K. (1997) *J. Neurosci.* **17,** 1596–1603
22. Hasegawa, H., Zinsser, S., Rhee, Y., Vik-Mo, E. O., Davanger, S., and Hay, J. C. (2003) *Mol. Biol. Cell* **14,** 698–720
23. Hay, J. C., Klumperman, J., Oorschot, V., Steegmaier, M., Kuo, C. S., and Scheller, R. H. (1998) *J. Cell Biol.* **141,** 1489–1502
24. Springer, S., and Schekman, R. (1998) *Science* **281,** 698–700
25. Rein, U., Andag, U., Duden, R., Schmitt, H. D., and Spang, A. (2002) *J. Cell Biol.* **157,** 395–404
26. Matsuoka, K., Morimitsu, Y., Uchida, K., and Schekman, R. (1998) *Mol. Cell* **2,** 703–708
27. Otte, S., and Barlowe, C. (2002) *EMBO J.* **21,** 6095–6104
28. Hay, J. C., Chao, D. S., Kuo, C. S., and Scheller, R. H. (1997) *Cell* **89,** 149–158
29. Laue, T., Shaw, B. D., Ridgeway, T. M., and Pelletier, S. L. (1992) in *Analytical Ultracentrifugation in Biochemistry and Polymer Science* (Harding, S. E., Rowe, A. J., and Horton, J. C., eds) pp. 90–125, The Royal Society of Chemistry, Cambridge, UK
30. Kweon, D. H., Chen, Y., Zhang, F., Poirier, M., Kim, C. S., and Shin, Y. K. (2002) *Biochemistry* **41,** 5449–5452
31. Margittai, M., Fasshauer, D., Pabst, S., Jahn, R., and Langen, R. (2001) *J. Biol. Chem.* **276,** 13169–13177
32. Xiao, W., Poirier, M. A., Bennett, M. K., and Shin, Y. K. (2001) *Nat. Struct. Biol.* **8,** 308–311
33. Misura, K. M., Gonzalez, L. C., Jr., May, A. P., Scheller, R. H., and Weis, W. I. (2001) *J. Biol. Chem.* **276,** 41301–41309
34. Chao, D. S., Hay, J. C., Winnick, S., Prekeris, R., Klumperman, J., and Scheller, R. H. (1999) *J. Cell Biol.* **144,** 869–881
35. Lippincott-Schwartz, J., Donaldson, J. G., Schweizer, A., Berger, E. G., Hauri, H. P., Yuan, L. C., and Klausner, R. D. (1990) *Cell* **60,** 821–836
36. Lippincott-Schwartz, J., Yuan, L. C., Bonifacino, J. S., and Klausner, R. D. (1989) *Cell* **56,** 801–813
37. Hay, J. C., Hirling, H., and Scheller, R. H. (1996) *J. Biol. Chem.* **271,** 5671–5679
38. Saraste, J., and Svensson, K. (1991) *J. Cell Sci.* **100,** 415–430
39. Laage, R., Rohde, J., Brosig, B., and Langosch, D. (2000) *J. Biol. Chem.* **275,** 17481–17487
40. Fasshauer, D., Otto, H., Eliason, W. K., Jahn, R., and Brunger, A. T. (1997) *J. Biol. Chem.* **272,** 28036–28041
41. Hanson, M. A., and Stevens, R. C. (2000) *Nat. Struct. Biol.* **7,** 687–692